Renewable Energy xxx (xxxx) xxx

Contents lists available at ScienceDirect

Renewable Energy

journal homepage: www.elsevier.com/locate/renene

Ground testing of a 1% gravo-aeroelastically scaled additively-manufactured wind turbine blade with bio-inspired structural design

Meghan Kaminski [a, *], Eric Loth [a], D. Todd Griffith [b], Chao (Chris) Qin [a]

[a] University of Virginia, Department of Mechanical and Aerospace Engineering, 122 Engineer's Way, Charlottesville, VA, 22904, USA
[b] The University of Texas at Dallas, Department of Mechanical Engineering, 800 W. Campbell, Richardson, TX, 75080, USA

ARTICLE INFO

Article history:
Received 4 November 2018
Received in revised form
1 October 2019
Accepted 28 October 2019
Available online xxx

Keywords:
Scaling
Wind turbines
Bio-inspiration
Additive manufacturing
Structural optimization

ABSTRACT

A gravo-aeroelastic scaling (GAS) method is developed to design wind turbine blades that represent centrifugal, aerodynamic, and gravitational loads of extreme-scale turbines. To match these elements, certain blade characteristics are given priority: non-dimensional 1st flap-wise frequency, non-dimensional flapping tip deflection, and tip-speed-ratio. Using the GAS method, a 1% sub-scale blade was designed to match the mass distributions and ground tested to match the non-dimensional flap-wise dynamics and deflections of Sandia National Lab's 13.2-MW blade. To the authors' knowledge, this is the first manufactured blade model to employ gravo-aeroelastic scaling using additive manufacturing and bio-inspiration. A series of scale models were designed, built, and ground-tested using weights consistent with scaled steady rated load conditions of an extreme-scale turbine. The models designed were evolved to increase gravo-elastic scaling performance by employing lightweight bio-inspirational morphology and carbon fiber reinforcements. The final version has non-dimensional gravo-elastic errors as follows: 3% in total mass, 15.6% in deflection from ground-based loads representing full-scale steady rated conditions, and 8.1% in the first flap-wise modal frequency (when normalized by the scaled rpm for rated conditions). This model demonstrates the GAS concept can be applied to manufacture sub-scale models as small as 1% of an extreme-scale rotor blade.

1. Introduction

In 2013, wind energy accounted for 4.5% of US electricity demand and is one of the fastest growing sources of new electricity supply [1]. It is predicted renewable energy will increase from 13% in 2013 to 18% in 2040 with wind being the largest source of renewable energy generation within the United States energy market [2]. The growth can be attributed to technology developments leading to an improvement of performance, an increase of reliability, and a reduction in the cost of energy [1]. Technological advances aid the increase in rotor diameter (D) and hub height (H) as seen in Fig. 1, with future turbines expected to have diameters in excess of 200-m and thus blade lengths in excess of 100-m.

Sandia National Labs has computationally shown this increase in blade size is viable with the design of the SNL100-XX series [3–6]. Each blade in the series is a 100-m blade designed for a 13.2 MW turbine. The initial baseline design, the SNL100-00 blade weighs 114 tons and is made primarily of fiberglass material with the conventional sharp trailing edge airfoil design of the time. The final design, the SNL100-03 blade, is the lightest version to satisfy all the key performance characteristics. It weighs 53 tons and uses carbon reinforcements and flatback airfoils to reduce the amount of material needed, which therefore reduces the weight compared to the initial design by over 50%. These turbines with blade lengths of 100-m and beyond have been termed "extreme-scale" systems [7].

Other turbine designs are also aiming for such extreme-scale rotors [7,8] however, due to the lack of physical testing on blades or rotors of this size, there are no experimentally confirmed designs as of yet [8]. Such full-scale testing (ground testing or field testing) is prohibitively expensive. As such, there is a need for scaled designs which can allow the physical testing to alleviate the risk of full-scale projects with new rotor technology [9]. In particular, scale models allow for verification of key aspects of blade and rotor design without the same commitment of resources [10].

Previous scaling techniques for structures under aerodynamic loads aim to scale aerodynamically and/or aeroelastically in order

* Corresponding author.
E-mail address: mek3xc@virginia.edu (M. Kaminski).

https://doi.org/10.1016/j.renene.2019.10.152
0960-1481/

Nomenclature

a_n	constant
a	speed of sound
$BSSE$	blade structural scaling error
c	chord length
c_t	distributed coefficient of thrust
D	average rotor diameter
d	diameter
EI	stiffness
g	gravitational constant
H	average hub height
I	sectional moment of inertia
L	beam length
m	blade mass
M	moment
M	a Mach Number
P	tip load
Re	Reynolds Number
s	spanwise location
S	total blade length
t	material thickness
U	wind speed
β	coning angle
δ	tip deflection
η	scaling factor
ρ	density
Ω	rotational speed
ω_{flap}	flap-wise frequency

Subscripts

$()_C$	centrifugal
$()_{cm}$	center of mass
$()_{design}$	version value
$()_f$	full-scale
$()_G$	gravitational
$()_i$	sectional value
$()_{ideal}$	ideal value
$()_{rated}$	rated value
$()_{rel}$	relative value
$()_s$	sub-scale
$()_T$	thrust
$()_{wind}$	wind value
$()$	distributed value
$\overline{()}$	non-dimensional value

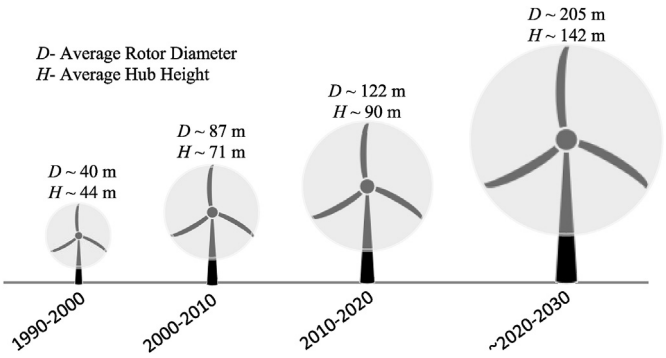

Fig. 1. The increasing trend of average production rotor sizes with the advancement of time.

to study deflection and dynamic responses suitable for validating computational methods [9–15]. These techniques have been used for testing helicopter blades [10], lightweight aircraft [11], and offshore wind turbines subjected to wave induced motions [9,12–15]. One such test, the DeepCwind test created a 1/50th-scaled model of a 5-MW offshore floating wind turbine [12,15]. The test utilizes Froude number scaling for the geometry and environmental conditions, and attempts to offset the changes in aerodynamic forces from the change in Reynolds number by increasing the windspeed. The turbines for this test properly scaled the mass of the turbine relative to the mass of the waves, however, the blades were made to be completely rigid in order to remove complications from stiffness scaling. This approach was appropriate as the interest was in understanding different floating platform designs and their interactions with an assortment of wind and wave loads and not on aeroelastic dynamics. In another example, a 1/93rd scaled wind turbine blade of the 44-m Vestas V90 blade was built to be aeroelastically scaled in terms of the ratio of flap-wise frequency to rotational frequency, but with the gravitational scaling ignored [13]. This approach was appropriate, as the interest was on the deflections caused by centrifugal and aerodynamic forces since gravitational loads are relatively small (in comparison) at rated conditions. However, scaling applied to extreme-scale turbines leads to additional complexity. In particular, gravitational loadings scale at a faster rate than aerodynamic loadings [3]. With blade lengths equal to or greater than 100-m, the gravitational loadings become of high significance [7,16,17] and therefore must also be taken into account. This indicates a need to apply a scaling which incorporates both the gravitational, aerodynamic, and elastic properties of wind turbine blades. While sub-scale designs have been completed [18], no such designs have been manufactured to the authors' knowledge.

Design and manufacturing difficulties arise if the scale reduction factor is significant. These difficulties include but are not limited to an extremely lightweight scaled mass, high stiffness, and the inability to manufacture the sub-scale with the same materials as the full-scale. These difficulties are further explained in the Methods section.

The mass and stiffness of a blade are limited when using the conventional skin and spar blade designs. To alleviate these limitations when scaling, a bio-inspired structural design is explored. It has been shown topologies resembling the internal structure of bone [19] can minimize mass, while withstanding a specified amount of load in a variety of directions. This structural efficiency follows Wolff's law, whereby human or animal bone structure grows and adapts to the loads applied and expected. Over time, if the bone's loadings increase, so will its internal support, if the loadings decrease, the support too will decrease [20]. The bone shown in Fig. 2a, includes many truss-like elements with rounded joining regions and with multiple directions of support. The concentration and size of these bone structures is specific to the applied and expected loads. As an example, someone highly active in a single-handed racquet sports can develop significant asymmetries between the bones of their dominant and non-dominant arms as compared to a control subject. This is a result of the increased loading on the racquet holding arm [21]. Thus, expected loads and evolutionary optimization allow for bone to have the lowest possible mass to support the given (applied or expected) loads. Inspired by such biological topologies, engineers use these

Please cite this article as: M. Kaminski et al., Ground testing of a 1% gravo-aeroelastically scaled additively-manufactured wind turbine blade with bio-inspired structural design, Renewable Energy, https://doi.org/10.1016/j.renene.2019.10.152

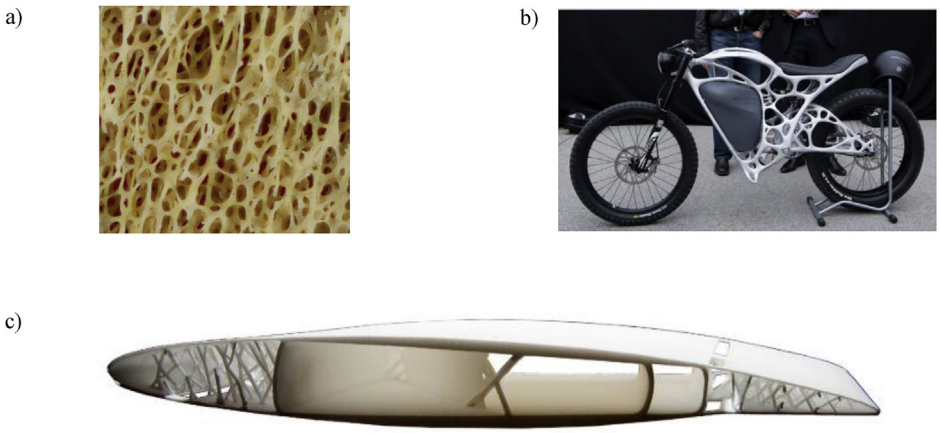

Fig. 2. a) Internal structure of the spongy bone in the femur of a cow [24], b) the first additively manufactured motorcycle [23,25], and the topologically optimized airplane wing [19].

structural concepts for product designs which must withstand a significant set of loads while retaining low mass. It is predicted this design technique will prove beneficial to the 1% model design.

Fabricating such bio-inspired designs with conventional manufacturing can be an extreme challenge, fortunately, additive manufacturing is an emerging technology allowing for separation from current subtractive methods by creating the product layer by layer. This allows for rapid innovative product design and testing without the need of extra spare parts, new tooling, etc. [22] which therefore reduces overall development cycles [23]. Additive manufacturing encourages novel product designs many of which resemble bio-inspired structural approaches to optimize the part's topology. Airbus's subsidiary, APWorks, is one of the leading designers in additively manufactured products. They have many different designs incorporating both bio-inspiration and additive manufacturing to reduce the weight and therefore the cost of the product. Among the many products are designs for an aircraft partition creating a 44% weight savings while also increasing the stiffness, a cabin bracket with a 72% weight savings, and an armrest with a 44% weight savings [23]. Their most unconventional part is the Light Rider motorcycle, the world's first prototype of a 3D printed motorcycle shown in Fig. 2b. Researchers at the Technical University of Denmark too are optimizing the internal structure of aircraft wings in order to reduce the mass compared to conventional as seen in Fig. 2c. These designs employ topologies similar to the internal bone topology of Fig. 2a. However, this concept has not been previously applied to a wind turbine blade structural design, which tend to favor more conventional skin-and-spar designs lacking the ability to further optimize the blade structural performance topology.

The first objective of this study is to combine both gravitational and aeroelastic effects for gravo-aeroelastically scaled models that allow for high-fidelity non-dimensional representation of the dynamics and deflections in the operation of extreme-scale rotors [16,17]. The second objective is to apply the GAS method to the SNL100-03 [6] wind turbine blade for a 1/100th structurally scaled model utilizing additive manufacturing and bio-inspired design. This model is then static ground tested with loads mimicking the full-scale steady rated conditions to show the viability of creating a model to simulate full-scale models at a sub-scale size.

To the authors' knowledge, this demonstration is the first study to additively manufacture and gravo-elastically test a scaled structural model of an extreme-scale wind turbine blade and the first to use the gravo-aeroelastic scaling method for design. Additionally, this is the first to employ bioinspired structural design to reduce weight for a given stiffness on scaled wind turbines.

Section 2 reviews the methods to obtain GAS models for extreme-scale wind turbine blades and methods to develop an additively manufactured blade displaying bio-inspired structural design. Section 3 includes the ideal scaling of the 1% SNL 100-03 blade used as a structural design goal and the physical iterations of the fabricated scaled blades seeking to replicate this ideal design via gravo-elastic ground testing. Section 4 provides concluding remarks and recommendations for future work.

2. Methods

2.1. Gravo-aeroelastic scaling

The following GAS method combines gravitational and aeroelastic scaling for an extreme-scale blade in terms of flap-wise structural performance to properly mimic the non-dimensional centrifugal, gravitational, and aeroelastic loads acting on the blade. To begin, it is important to determine a scaling factor of the model (η). This is defined by the ratio of the total blade lengths (S) shown in equation (1) and in Fig. 3a with the subscripts s and f referring to the sub-scale and full-scale models respectively. This factor also applies to all external dimensions and deflections of the blade including the center of gravity and the blade chord (c).

$$\eta = \frac{S_s}{S_f} \tag{1}$$

When scaling a blade, it is important to keep the blade root moments imparted at the rotor hub on the turbine scaled appropriately for the purpose of loads matching between full- and sub-scale. The moments experienced by the scaled blade determine the appropriate structural design and stiffness to preserve the non-dimensional deflections and dynamics of the full-scale blade. Because moments are influenced by forces with moment arms, this scaling places more emphasis on the loading and properties near the tip of the blade as compared to those inboard. The moments at the hub are expressed as a summation of all the distributed moments, which are the moments per unit spanwise length at a given point along the blade.

Fig. 3b depicts the blade in a vertical upward orientation with a coning angle (β) in order to express the distributed moments in the blade flap-wise directions for accurate tip deflections. The three main flap-wise distributed moments felt at the blade root are thrust

Please cite this article as: M. Kaminski et al., Ground testing of a 1% gravo-aeroelastically scaled additively-manufactured wind turbine blade with bio-inspired structural design, Renewable Energy, https://doi.org/10.1016/j.renene.2019.10.152

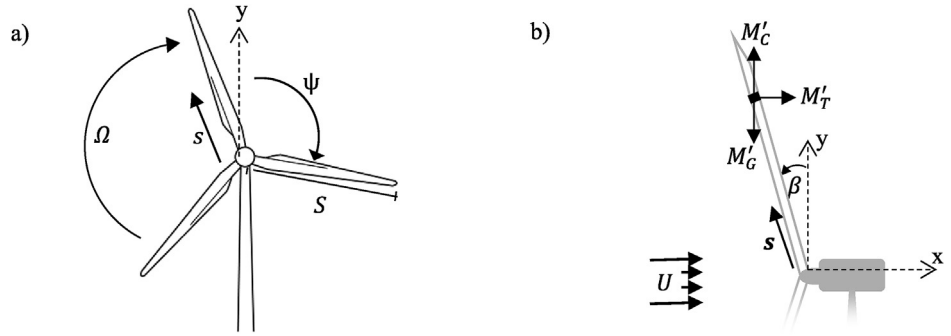

Fig. 3. An upwind three-bladed turbine with a) the front view showing: rotational speed (Ω), sectional distance along the blade length (s), and total blade length (S) and b) the side view showing sectional bending moments (M_Q), coning angle (β), and wind speed (U) and again the sectional distance along the blade length (s) with a non-rotating coordinate frame.

($M_T^{'}$), centrifugal ($M_C^{'}$), and gravitational ($M_G^{'}$). These are expressed analytically as follows:

$$M_T^{'} = \frac{1}{2}\rho_{wind} c U_{rel}^2 c_t s[cos(\beta)] \tag{2}$$

$$M_C^{'} = m^{'}\Omega^2 s^2[\cos(\beta)sin(\beta)] \tag{3}$$

$$M_G^{'} = m^{'}gs[sin(\beta)\cos(\psi)] \tag{4}$$

The values above include ρ_{wind} as the air density, U_{rel} as the relative wind speed (which includes wind speed due to the rotation of the blade and the incoming wind), Ω as the rotational speed, and g as the gravitational constant. The values that vary as a function of spanwise length, s, include c_t as the sectional coefficient of thrust, c as the chord length, and m' as the distributed mass density of the blade (with units of mass per unit spanwise length).

To find the total moments felt by the root of the blade, the sectional moments due to a force Q can be integrated from the root to the tip of the blade over a differential blade length (ds) as shown below, where Q can be replaced by C, T, or G.

$$M_Q = \int_0^S M_Q^{'} ds \tag{5}$$

There are two main moment ratios to define before determining the scaling parameters. The first is the ratio of sectional gravitational to centrifugal moments, which is the moment equivalent to the Froude number, and the second is the sectional centrifugal to thrust moment, where these are written as follows:

$$M_G^{'}/M_C^{'} = \frac{g}{\Omega^2 s[cos(\beta)]} \tag{6}$$

$$M_C^{'}/M_T^{'} = \frac{2m^{'}\Omega^2 s[sin(\beta)]}{\rho_{wind} c U_{rel}^2 c_t} \tag{7}$$

In terms of dynamics, aeroelasticity, and velocity angles, there are three critical non-dimensional values that should be held constant between the full- and sub-scale blades when designing the sub-scale model: the non-dimensional 1st flap-wise frequency, the non-dimensional maximum steady state tip deflections, and the tip-speed-ratio (TSR). The non-dimensional flap-wise frequency is defined in equation (8a). This is the ratio of the primary blade natural frequency (ω_{flap}), defined in equation (8b), based upon uniform beam deflections, to the primary input frequency (Ω, rotational speed). In this equation, α_n is a constant that is a function of boundary conditions, mass distribution, and stiffness distributions and is ideally the same between full- and sub-scale, EI is blade stiffness, m is total blade mass, and S is the length of the blade. This non-dimensional frequency drives the flap-wise dynamics of the blade and preserving this value ensures the scaled mass and stiffness values are proportional to each other. In addition, the flap-wise frequency divided by omega in equation (8a) is held constant from full-scale to sub-scale ensuring that the spacing of per-rev frequencies are maintained at sub-scale; for example, a design free of blade resonant conditions at the full-scale is also free of resonance at the sub-scale. The non-dimensional maximum steady state tip deflection defined in equation (9) is the ratio of the maximum steady-state rated deflection of the blade (δ) to the total length of the blade (S). A consequence of matching both equations (8a) and (9) is the scaled mass and stiffness will both be appropriately scaled. Lastly, by keeping the tip-speed-ratio (TSR) in equation (10) constant, the approaching flow angles relative to the rotor blade will be preserved. The various parameters within the TSR are visually shown in Fig. 3 where $\Omega Scos(\beta)$ is the tip-speed, and U is the wind speed.

$$\overline{\omega} = \frac{\omega_{flap}}{\Omega} \tag{8a}$$

$$\omega_{flap} = \alpha_n^2 \sqrt{\frac{EI}{mS^3}} \tag{8b}$$

$$\overline{\delta} = \delta/S \tag{9}$$

$$TSR = \frac{\Omega Scos(\beta)}{U} \tag{10}$$

Keeping equations (8a), (9) and (10) constant, the scaling of appropriate blade parameters are determined using equations (1)–(4). The factors are summarized in Table 1, and the steps used to obtain them are as follows.

To begin, the rotational speed scaling ($\eta^{-1/2}$) is found by keeping the ratio of equation (6) constant between full- and sub-scale and applying the scaling factor of equation (1). With this result and keeping the tip-speed-ratio constant in equation (10), the wind speed scaling ($\eta^{1/2}$) is obtained. Applying the scaling factor to both the chord and to the sectional blade length, as well as scaling the wind and rotational scaling by equation (7), the distributed blade mass scaling can be obtained. The result for the distributed blade mass scaling is η^2 if the air density does not vary, but if the full-scale and sub-scale systems operate at substantially different altitudes, then air density effects should be considered. From this, one can

Please cite this article as: M. Kaminski et al., Ground testing of a 1% gravo-aeroelastically scaled additively-manufactured wind turbine blade with bio-inspired structural design, Renewable Energy, https://doi.org/10.1016/j.renene.2019.10.152

Table 1
Various parameters for GAS scaling and their associated scaling factors.

Scaling Parameter	Scale Factor
Length Scaling: $\frac{S_s}{S_f}$	η
Rotational Scaling: $\frac{\Omega_s}{\Omega_f}$	$1/\sqrt{\eta}$
Wind Velocity Scaling: $\frac{U_s}{U_f}$	$\sqrt{\eta}$
Total Blade Mass Scaling: $\frac{m_s}{m_f}$	$\left(\frac{\rho_{wind,s}}{\rho_{wind,f}}\right)\eta^3$
Distributed Blade Mass Scaling: $\frac{m_s^{'}}{m_f^{'}}$	$\left(\frac{\rho_{wind,s}}{\rho_{wind,f}}\right)\eta^2$
Flap-wise Frequency Scaling: $\frac{\omega_{flap,\,s}}{\omega_{flap,\,f}}$	$1/\sqrt{\eta}$
Stiffness Scaling: $\frac{(EI)_s}{(EI)_f}$	$\left(\frac{\rho_{wind,s}}{\rho_{wind,f}}\right)\eta^5$
Reynolds Number Ratio: $\frac{Re_s}{Re_f}$	$\left(\frac{\rho_{wind,s}}{\rho_{wind,f}}\right)\left(\frac{\mu_{wind,f}}{\mu_{wind,s}}\right)\eta^{3/2}$
Mach Number Ratio: $\frac{Ma_s}{Ma_f}$	$\left(\frac{a_{wind,f}}{a_{wind,s}}\right)\sqrt{\eta}$
For Fixed Materials and Structural Design:	
Material Thickness Scaling: $\frac{t_s}{t_f}$	$\left(\frac{\rho_{wind,s}}{\rho_{wind,f}}\right)\eta^2$

integrate to obtain the total blade mass scaling (η^3). With keeping the non-dimensional flapping frequency constant in equation (8a) and applying the rotational scaling previously determined, one obtains the scaling for the flap-wise frequency ($\eta^{-1/2}$). Applying the scaling for frequency, mass, length, and the assumption that the α_n term of equation (8b) remains constant between the full- and sub-scale models, the bending stiffness (EI) scaling can be obtained (η^5). When developing a scaled model with the same materials, the wall thickness scales by combining the stiffness scaling and the moment of inertia of a section. For example, the sectional moment of inertia for a hollow uniform circle of diameter, d, and wall thickness, t, is given as follows:

$$I = const.\left(d^3 t\right) \tag{11}$$

This same proportionality (with a different defined constant) applies for a wind turbine blade given a reference diameter and blade skin thickness. Assuming material similarity at full- and sub-scale the sectional moment of inertia, equation (11), scales with η^5 (assuming all material properties are unchanged), thus the material thickness is to be scaled by η^2, as opposed to the assumed scaling, η, in order to preserve the scaled blade stiffness.

When scaling in the same fluid density, there will be a difference in Reynolds number and Mach numbers. The difference in Mach number can be reasonably ignored if the Mach numbers are below compressibility effects [11]. For the Reynolds number mismatch, studies have shown the aerodynamics can be sensitive to such changes so that fixing the aerodynamic shape and flow angles will not preserve the thrust coefficient [26]. It should be noted that the objective of scaling flap-wise loads is to achieve the same moment ratios and overall aeroelastic loads. Thus, one may design the sub-scale model at a different C_p and change the pitch to match the thrust coefficient and flap-wise dynamics at a single operating point. Additional options to better match the thrust include, but are not limited to: tripping the boundary layer, redesigning the airfoil geometry, and applying an appropriate resisting motor to the turbine [16,27,28]. Note that matching the scaled flap-wise moments with such changes will generally prevent simultaneous scaling of the edgewise moments. However, the flap-wise deflections and dynamics are the focus herein as they are much greater than the corresponding edgewise values for the full-scale turbine. As such, the decision for adjustments is dependent on specific research goals.

2.2. The SNL100-03 blade reference design

In the present study, the GAS method is applied to the 13.2 MW 100-m SNL100-03 wind turbine blade [6] to determine a 1% model. This full-scale blade model is chosen based upon its advanced design as an extreme-scale wind turbine. The SNL100-03 is a fourth generation concept design [3–5] that introduces flatback airfoils to reduce the weight of the blades and includes the following blade materials (by percent of the total blade mass): E-Glass/Epoxy (E-LT-5500) - 15.5%, Saertex - 11.4%, Carbon Prepreg - 30.1%, Epoxy Resin (EP-3) - 32.5%, Balsa - 2.5%, Polyethelene Teraphalate (PET) Foam - 6.5%, and a Gel coat - 1.3%. The primary materials are located in Fig. 4 which also depicts the internal structure of the full-scale SNL100-03 blade including the shear webs and the upper and lower spar caps [6].

2.3. Scaled model ground-testing method

To assess whether the GAS method can be successfully applied

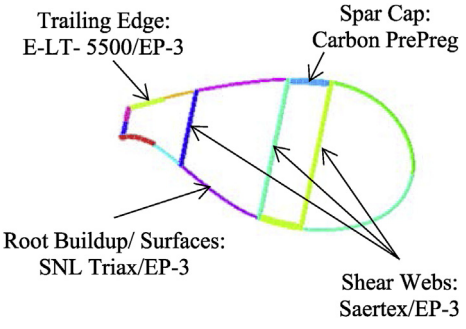

Fig. 4. The primary structure and materials of the full-scale SNL100-03 blade.

Please cite this article as: M. Kaminski et al., Ground testing of a 1% gravo-aeroelastically scaled additively-manufactured wind turbine blade with bio-inspired structural design, Renewable Energy, https://doi.org/10.1016/j.renene.2019.10.152

to models as small as 1/100th scale, equations (8a)-(10) are verified in terms of the gravo-elastic properties. In particular, ground testing is used to compare the blade mass (sectional distribution as well as total value), maximum steady state tip deflection, and first flap-wise frequency of the blade. Other aspects are of secondary influence on flap-wise deflections and thus are not scaled: the chord wise mass density, edgewise stiffness, rotational stiffness, and axial stiffness. These are secondary since the primary forces which impact blade flap-wise deflections for the full-scale rotor in operation are flap-wise gravitational, aerodynamic, and centrifugal forces. The total mass of a manufactured blade is obtained through weighing on a scale, accurate to ±0.1 g, while the mass density (mass per unit span) is verified through SOLIDWORKS. The center of mass is also compared between the full- and sub-scale models through equation (12) and summing down the length of the blade.

$$s_{cm} = \frac{\sum s_i m_i}{m} \tag{12}$$

Typical aeroelastic testing involves an interaction between the aerodynamic, elastic and inertial forces on a structure in a flow. Such operational testing for a study of this scale can be very difficult since, the Reynolds number mismatch can significantly affect the aerodynamics. Therefore, the blades are only static ground tested for flap-wise tip deflections by applying weights to represent the scaled operational root flap-wise bending moment at steady rated conditions. Fig. 5 shows the setup for testing the tip-deflection and the first flap-wise frequency of the blade. The root of the blade is held in place creating a fixed root boundary condition. For testing of the maximum steady state tip deflection, various loads stepping up to the maximum scaled flap-wise moment of the full-scale blade are applied to the tip and the amount the tip deflects is measured from a static state shown in Fig. 5c. This is compared to non-dimensional ANSYS deflections of the SNL100-03. Although the stiffness along the length of the blade varies, the maximum tip deflections (δ) are similar to a uniform, constant stiffness (EI) beam of length L, resulting from a tip load (P) as described in equation (13).

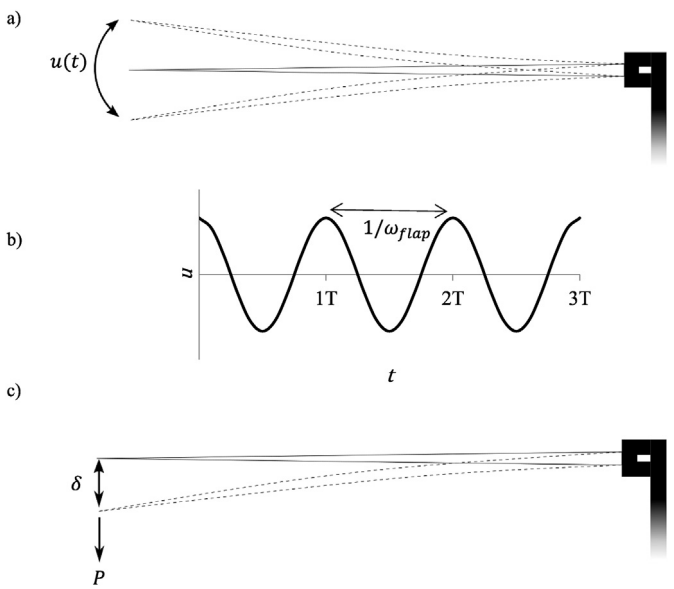

Fig. 5. The experimental setup to test scaled blade deflections: a) unsteady deflections resulting from a pluck test, b) time evolution of deflections to obtain natural frequency, and c) steady state tip deflections based on a scaled load placed at the tip.

$$\delta = \frac{PL^3}{3EI} \tag{13}$$

This flap-wise deflection in a gravo-elastic ground test can be used to quantify the steady-state scaling properties of the fabricated blade. In particular, this deflection can be normalized by blade length to compare with the non-dimensional deflection values of the full-scale blade by using Table 1.

To consider the dynamic properties of this same blade, a step relaxation, or "pluck test", is applied to determine the first flap-wise frequency shown in Fig. 5a. This is achieved by applying a fixed load to the tip of the blade, and then removing it suddenly so the blade responds in an unsteady manner with free vibrations [29]. The flap-wise frequency of the blade is determined by the inverse of the time for the blade to complete one cycle of deflections as described by Fig. 5b. These vibrations can be used to determine flap-wise frequency and can be compared to the non-dimensional values of the full-scale blade by using Table 1.

2.4. Scaled model materials, manufacturing and scaling accuracy parameter

For manufacturing the 1/100th model, the material thickness-scaling factor from Table 1 is referenced. When scaling the familiar material of balsa at its maximum thickness of 39 mm, the 1% scaled model operating in the same air density would be 3.9 μm. This is an impractically small thickness (the thinnest available piece of balsa readily available for production is 0.5 mm) and one that would lead to buckling problems. Therefore, alternate materials and structural designs are needed to manufacture the scaled blade. Additive manufacturing of the blade was determined to be a highly effective solution for design since it allows for quick turnaround time between the design phase and the manufacturing phase [30]. Another benefit of additive manufacturing is the additional degrees of freedom of design topography as compared to subtractive manufacturing methods [31] permitting innovative structural designs and the ability to match the structural efficiency of the full-scale at a sub-scale size.

For the 1/100th blade, the Stratasys PolyJet 3D printer was used due to its ability to print multiple materials on a single part, high tolerance, layer resolution, and accuracy [32]. The PolyJet 3D printer allows for the combination of materials utilized for manufacturing as outlined in Table 2. This range of material stiffness allows alterations in the deflections similar to the beam deflection equation (13) and can help to retain the main values outlined in equations (8a), (9) and (10). Additional materials such as a carbon fiber strip (for added blade stiffness) and the plastic wrap (for external blade shell) are also included in Table 2.

Additive manufacturing presents limitations to the wall thickness. With this limitation, and the mass constraints presented in Table 1, the third shear web is removed through all iterations of the blade. The goal is to keep the remaining internal structure of the blade constant with the full-scale model; however, if needed, the internal structure can be altered so long as the blade retains the main values outline in equations (8a), (9) and (10). Even with the removal of the third shear web, structural optimization is required to satisfy these values at the subscale due to the low mass and high stiffness constraints of extreme-scale wind turbines.

Conventional manufacturing techniques at the sub-scale cannot match the full-scale blade dynamics due to design limitations in both the mass and stiffness constraints. Optimization of the structure to match these constraint requirements (such as stress, structural deflection, mass, etc.), is completed by reducing the mass and material within a given outer shape [36,37]. The optimized

Please cite this article as: M. Kaminski et al., Ground testing of a 1% gravo-aeroelastically scaled additively-manufactured wind turbine blade with bio-inspired structural design, Renewable Energy, https://doi.org/10.1016/j.renene.2019.10.152

Table 2
Material properties of the elements for the 1% GAS SNL100-03 blade.

Material	Vendor & Name	Modulus of Elasticity (MPa)	Density (g/cm^3)
Rigid Resin	Stratasys- VeroWhite	2100	1.17
Rigid + Rubber Resin	Stratasys- RGD8505	1900	1.17
Rigid + Rubber Resin	Stratasys- RGD8510	1700	1.17
Rigid + Rubber Resin	Stratasys- RGD8515	1500	1.17
Rigid + Rubber Resin	Stratasys- RGD8520	1300	1.17
Rigid + Rubber Resin	Stratasys- RGD8525	1000	1.17
Rigid + Rubber Resin	Stratasys- RGD8530	700	1.17
Rubber Resin	Stratasys- Tango Black	~5.8	1.14
Carbon Fiber	The Composites Store- High Modulus Carbon Fiber Strip [33]	240000	1.59
Polyethylene	GLAD ClingWrap [34,35]	~113	1.68

structures lead to designs with high stiffness, low mass, and designs with material solely in locations where it is needed, and voids where material is not needed. This design methodology is known as a bio-inspired structural design [37]. To test the efficiency of the design, a Blade Structural Scaling Error (BSSE) is defined for comparison with previous designs. For the case of the 1% blade, the design performance is based upon the tip deflections and the mass of the blade as defined in equation (14). If the BSSE is 0, then the stiffness and mass is scaled appropriately, and therefore the blade frequency (by Equation (8b)) is also scaled appropriately.

$$BSSE = \sqrt{\left(\frac{\delta_{design} - \delta_{ideal}}{\delta_{ideal}}\right)^2 + \left(\frac{m_{design} - m_{ideal}}{m_{ideal}}\right)^2} \tag{14}$$

To reduce the BSSE of the design, the structure must closely match the mass and deflections of the full-scale model. To match each of these, it is intelligent to refer to the way in which the internal structure of bone is developed, namely, the spongy bone. This keeps the mass as low as possible, while also being able to withstand the given loadings resulting in an internal structure resembling Fig. 2a. By replicating and adapting this design, the 1% model will ideally be able to match the difficult mass constraints of a scale model of this size, but also be able to match the tip deflections prescribed ultimately reducing the BSSE of the blade.

3. Results and discussion

3.1. Gravo-aeroelastic scaling results

Applying the GAS methods of Table 1 to a 1/100th model of the SNL100-03 blade results in the scaling summarized in Table 3. The leftmost column contains the full-scale 100-m values, the middle column contains the GAS scaled 1% values and, to compare extreme-scale values to conventional values, the rightmost column contains a conventional 0.9-m length blade [38]. The conventional rotor mass, even though it uses fiberglass and carbon fiber, is about 4.5 times heavier than the sub-scaled version of an extreme-scale rotor of about the same length. This difference shows gravo-aeroelastic sub-scaling dramatically reduces the blade mass relative to what would be expected from a technology used for similar blade lengths. This is demonstrated in Fig. 6 which shows the trends in mass scaling for gravo-aeroelastic scaled blades and conventional blades. The solid black line shows typical blade mass for rotors designed ideally for their respective size, and shows the SNL100-03 blade is consistent with this trend. This trendline shows mass changes with $S^{2.1}$ due to differing technological evolutions including manufacturing techniques and materials as blade rotor sizes increase. This proportionality is well documented [39,40]. The dashed blade line shows the mass of a blade scaled gravo-aeroelastically, following an S^3 line (Table 3). Using the SNL100-

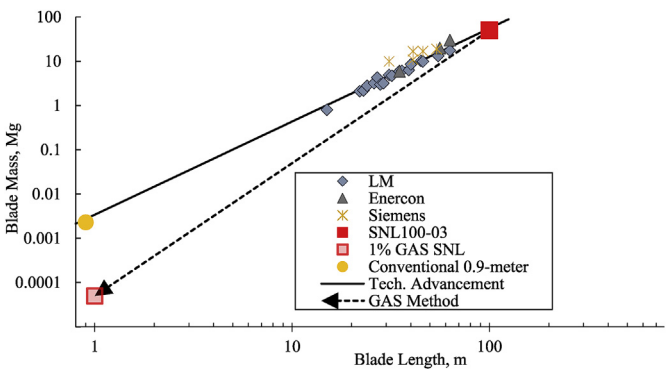

Fig. 6. The technological advancement of blades (solid line) compared against GAS method blades (dashed line).

Table 3
The 1% Ideal GAS SNL100-03 blade and its full-scale counterpart compared to a conventional blade.

	Full-Scale SNL-100-03	1% Ideal GAS SNL100-03	Carbon Fiber 0.9-Meter Blade [38]
Design Innovation	Extreme-Scale	Extreme-Scale	Conventional-Scale
Rotor Radius (R)	100 m	1 m	0.9 m
Length Scaling Factor (η)	1	0.01	–
Blade Mass (m)	49,519 kg	49.52 g	220 g
Rated Wind Speed (V_{rated})	11.3 m/s	1.13 m/s	12.5 m/s
Tip-Speed Ratio (λ)	9.5	9.5	11.6
Rated Rotor speed (Ω)	10.25 RPM	102.5 RPM	649 RPM
Flap-wise Frequency (ω_{flap})	0.49 Hz	4.9 Hz	–
Ref. Reynolds Number (Re)	1.54×10^7	1.23×10^4	4.14×10^5
Ref. Mach Number (Ma)	0.224	0.022	0.119

Please cite this article as: M. Kaminski et al., Ground testing of a 1% gravo-aeroelastically scaled additively-manufactured wind turbine blade with bio-inspired structural design, Renewable Energy, https://doi.org/10.1016/j.renene.2019.10.152

03 blade as the reference, a 1-m gravo-aeroelastic blade is significantly lighter than a blade using conventional technologies at the same length. This highly reduced mass required for the gravo-aeroelastically scaled blade demonstrates a challenge of creating a very low mass design as compared to designs using conventional methods.

The primary reasons for the reduced blade mass when GAS is applied is illustrated in Fig. 7, which shows the ratio of the moment due to gravitational loads to the moment due to centrifugal loads M_g/M_c. The solid black line again shows the conventional values for this ratio based on an assumption of constant tip-speed, which results in gravitational moments being much weaker at small scales. The dashed black line shows the constant value of this moment ratio needed to properly employ the GAS method including changes in tip-speed (Table 1). This plot shows the significance of gravitational loading for extreme-scale blades. In the following, various structural designs are considered in order to keep this moment ratio of Fig. 7 constant with the low mass shown in Fig. 6.

3.2. Iterations of 1% GAS SNL100-03 blade

The structural design iterations of the 1% GAS SNL100-03 blade are rendered in Fig. 8 with mass and deflection summarized in Table 4. The different iterations start with Version 0 and lead up to the final blade design of Version 5CF. The Version 0 blade mimics the full-scale conventional skin-and-spar structural design excluding the third shear web (as mentioned in Section 2.4) and is far too heavy even if fabricated with the minimum thickness material allowed by additive manufacturing (it would weigh about 122 g, which is 2.46 times more than ideal weight). As such, the blade was never fabricated and its high mass highlights the need to explore structural optimization and non-conventional geometries.

To design the structure to minimize the mass and maximize the stiffness, it is important to take into account both the aerodynamic shape of the blade as well as the structural loadings on the blade [41,42]. If only focusing on the aerodynamics, the resulting blade would be a solid blade with an aerodynamic shell. If only focusing on the structure of the blade, the resulting shape would be an I-beam with no external airfoil. Therefore, to fully optimize the blade for mass and stiffness, material must remain where loads act upon it and be removed where loads do not act upon it while simultaneously providing support for the outer shell to retain aerodynamic shape. In terms of material that must remain, the leading edges and trailing edges were unaltered due to their critical influence on aerodynamics [44]. Each design version presented is based upon authors' experience and the previous design results. In terms of material that could be removed, oval holes were employed on the upper and lower surfaces. The rounded corners reduce the stress concentrations as compared to the sharp corners if squares were removed [43] and the removed ovals are spaced evenly down the length of the blade to provide support for the outer shell, polyethylene wrap. This set of design decisions led to structural designs and methodologies similar to the spongy bone of Fig. 2a, and therefore a bio-inspired structure.

The Version 1 blade takes the same shear web internal structure as Version 0, but removes material in the outer shell. This results in a blade with reasonable stiffness, but still too high of a mass (nearly 50%). The following discusses the remaining structural designs that attempt to match both the mass and stiffness with Table 4 summarizing the ground testing results, design considerations, and design successes. The remainder of the design versions are based upon manufacturing iteration and assessment with an emphasis on bio-inspiration.

Since the structural design of Version 1 yields too large of a mass, the Version 2 blade removes mass in the spar, also in the shape of ovals, down the length of the blade. This blade is printed with a stiffer material to offset the removal of this material. While there was improvement in the mass of the blade, it is still too massive, deflects too little, and has significantly lower edgewise stiffness (though, edgewise stiffness is not a priority in the present GAS approach) as summarized in Table 4.

Version 3 blade sought to improve upon Version 2 by further invoking a bio-inspired internal structure. The shear webs are widened and rounded and the sizes of the empty spaces are increased in both the external and internal structure. This results in a much-improved mass similar to the ideal blade. However, even when printing with the stiffest material available, the blade is too flexible in the flap-wise direction. In order to increase this stiffness, a carbon fiber strip is superficially attached on the suction side of the blade similar to previous blade designs [13]. This design is denoted as Version 3CF, with the inclusion of carbon fiber indicated by the 'CF'. This addition of carbon fiber significantly increases the stiffness with little mass increase. Succeeding iterations continue to contain a carbon fiber strip. However, further iterations were needed as this blade was too stiff (tip deflection was too small) and too heavy.

Version 4CF employs the carbon fiber, as in Version 3CF, but uses a structure similar to Version 2, except with a singular shear web and a track for placement of the carbon fiber strip. This results in a blade with mass close to the ideal scaled mass, but a stiffness that is too high. Version 5CF continues with the same design, however the

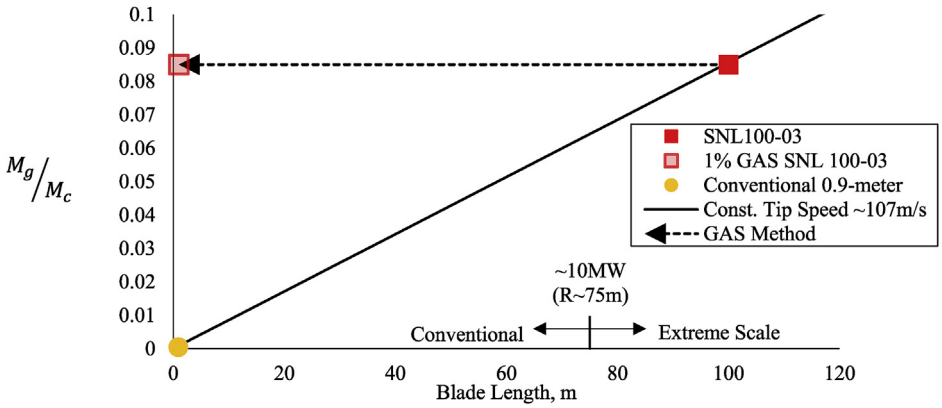

Fig. 7. Ratio of gravitational to centrifugal moments using GAS methods as shown by the dashed line, where the solid diagonal black line is based on a fixed tip speed (~107 m/s) and as-fabricated blade masses.

Please cite this article as: M. Kaminski et al., Ground testing of a 1% gravo-aeroelastically scaled additively-manufactured wind turbine blade with bio-inspired structural design, Renewable Energy, https://doi.org/10.1016/j.renene.2019.10.152

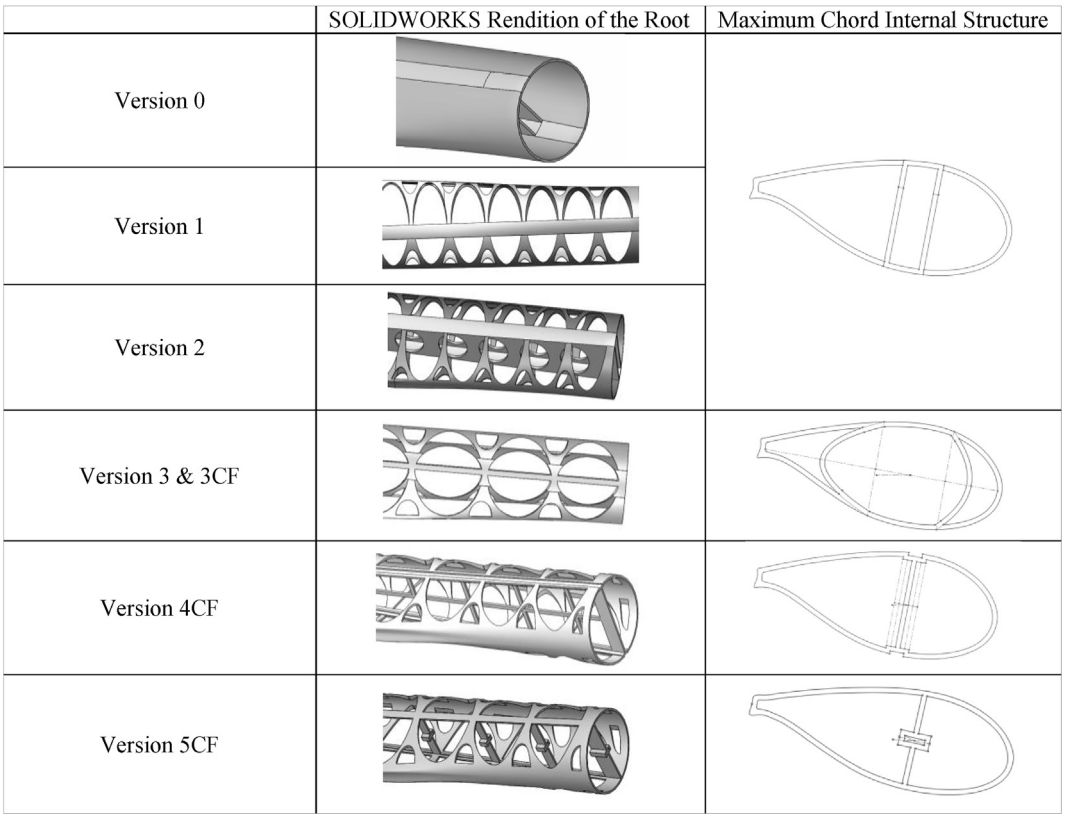

Fig. 8. Design iterations of the 1% GAS SNL100-03 blade.

Table 4
Results of the fabricated 1% GAS SNL blades, by version iteration.

1% GAS SNL Version	Mass (g)	Max. Flap-wise Steady State Tip Deflection (cm)	Primary Material	Design Changes	Design Effect
Ideal	49.5	19.5	(–)	(–)	(–)
Version 1	69.2	17.9	Spar: RGD8530 Lead and Trailing Edges: RGD8525	Material removed from outer surface, full-scale internal structure	Reasonable flap-wise stiffness, too massive
Version 2	65.4	10.0	Spar: RGD8515 Lead and Trailing Edges: RGD8520	Material removed from spar, stiffer material	Too stiff flap-wise, too massive, significantly low edge stiffness
Version 3	54.2	23.3	VeroWhite	Widened spar, stiffest material	Too flexible flap-wise, reasonable mass
Version 3CF	56.2	9.8	VeroWhite	Superficial carbon-fiber spanwise strip	Too stiff flap-wise, reasonable mass
Version 4CF	52.0	7.3	VeroWhite	Single straight spar, carbon fiber on suction side	Too stiff flap-wise, reasonable mass
Version 5CF	51.0	16.45	RGD8505	Less stiff material, single straight spar, carbon fiber down center	Reasonable flap-wise stiffness, reasonable mass

carbon fiber placement has been shifted to the middle of the blade. Although the carbon fiber is near the neutral axis (providing minimal changes to the blade inertia), the material stiffness is ~100 times greater than the Polyjet 3D printed materials causing a significant increase in stiffness as compared to a model with no carbon fiber included. The final Version 5CF blade has a total mass error of +3% and a gravo-elastic tip deflection error of −15.6%. The design evolution errors for both the total mass and flapping tip deflection are shown in Fig. 9 with positive values referring a high mass and deflection.

To quantify the net improvement in structural design through iteration, the BSSE values (equation (14)) are shown in Fig. 10. As a reminder, the BSSE combines the mass and deflections errors of the designed model, to the ideal model. The closer the BSSE is to zero, the better the design. It can be seen that large changes in structural

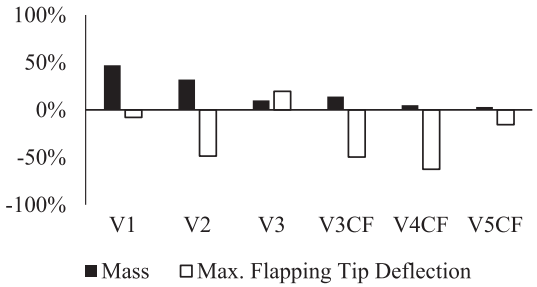

Fig. 9. Percent difference from scaled values of the SNL100-03 blade of the total mass and maximum steady state tip deflection. Positive values are greater than the target, negative values are less than the target.

Please cite this article as: M. Kaminski et al., Ground testing of a 1% gravo-aeroelastically scaled additively-manufactured wind turbine blade with bio-inspired structural design, Renewable Energy, https://doi.org/10.1016/j.renene.2019.10.152

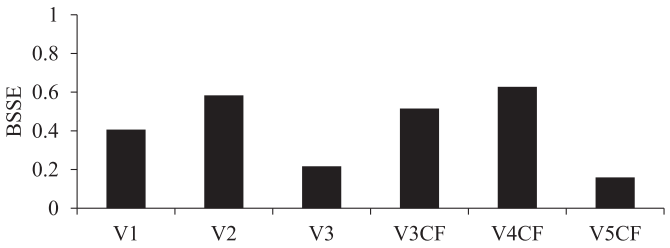

Fig. 10. The Blade Structural Scaling Error for the design iterations of the 1% GAS SNL100-03 blade which all utilize Polyjet 3D print materials and polyethylene wrap while the final three versions (denoted with the CF) also contain carbon fiber strips.

design did not necessarily reduce the BSSE but allowed for improvements towards the final version, which subsequently had the lowest BSSE. For example, the increase between Version 3 and Version 3CF, is due to the addition of the carbon fiber and helped drive the BSSE to its lowest value for Version 5CF. If the BSSE is zero, then the mass and stiffness of the blade natural flap-wise frequency can be expected to have scaled appropriately. As such, frequency was only measured for the final blade iteration, as discussed below.

3.3. Final version of 1% scaled blade

The top view of the final version (5CF) of the scaled wind turbine blade is shown in Fig. 11. The blade design has similar characteristics as the bone structure in Fig. 2a. As noted above, this blade has similar total mass and tip deflection properties, which would suggest that flap-wise frequency and stiffness distributions would also be reasonable. The idealized scaled natural flap-wise frequency is 4.9 Hz as shown in Table 3. The frequency of the 1% GAS SNL100-03 blade was measured with the technique shown in Fig. 5a and b, which yielded 4.5 Hz, an 8.1% decrease from ideal.

Fig. 12a depicts both a portion of the physically printed 1% GAS SNL100-03 blade, and Fig. 12b shows the blade linear mass density (mass per unit span) over the length of the blade. Since the design has many local variations in the organic structure, the linear density (red squares) oscillates significantly. When these values are smoothed out to get a representative linear density distribution (the red dashed line), the result is similar to that of the ideal scaled values shown as the black solid line. Using the smoothed mass density and equation (12) for the radial center of mass of the blades, the full-scale center of mass is at 31.5% span and Version 5CF slightly more outboard at 40.7% span. This difference can be attributed to the higher mass density near the tip of the blade as seen in Fig. 12b.

Fig. 13 shows the deflection of the full-scale and sub-scale blade when loaded in the static pull test (Fig. 5c) with an applied moment using weights, which is consistent with steady-state rated operational conditions. The fabricated and full-scale shapes are similar inboard; however, the scaled blade is too stiff outboard yielding a smaller tip deflection. This is consistent with deflections at the tip of the blade as shown in Fig. 14 for a range of loads up to the steady-state conditions.

The model deflection being 15.6% too low, correlates to the stiffness being 18.4% too high when following the trends of equation (13). This stiffness increase and the mass increase of 3.0%, applied to equation (8b), results in an increased predicted frequency error of 7.2%. However, the measured frequency is 8.1% too low. This can be attributed to the center of gravity being 9.0% farther out on the span. To improve upon the model, future iterations can remove additional material from outboard on the blade to reduce total mass, reduce outboard mass density, move the center of gravity inboard, and reduce outboard blade stiffness. These consequences may additionally increase the blade natural frequency closer to the target.

4. Conclusions and recommendations

The current study presents a unique approach to structurally scaling wind turbine blades using the gravo-aeroelastic scaling (GAS) method applied to a blade from an extreme-scale turbine (rated at 13.2 MW) to design a 1/100th scale model. The method allows for a low-cost fabricated model that can reflect the proper non-dimensional flap-wise dynamics and elastic deflections of the full-scale blade. The scaling was achieved by reasonably reproducing the non-dimensional flap-wise frequency, tip-deflection, deflection shapes and linear mass density distributions of the full-scale model. Notably, the scaled model requires extremely light mass while maintaining proper stiffness. This was achieved via additive manufacturing, structural designs inspired by bone growth, and the stiffness reinforcement of a carbon fiber spar. The scaling performance of the various blade structural designs were evaluated through gravo-elastic ground tests and quantified by the Blade Structural Scaling Error which considers the differences in total blade mass and blade deflections. The final blade had the lowest BSSE of 0.16 which is based on a 3% mass error and a steady flap-wise tip deflection error of 15.6%. This design also had an 8.1% error in flap-wise frequency and reasonable representation of linear mass density. However, the model was higher than ideal near the tip causing the center of mass of the blade to be more outboard (at 40.7% span as opposed to ideal at 31.5% span).

Recommendations for future work include the application of the GAS method to field-tested sub-scale rotors to investigate their ability to describe full-scale gravo-aeroelastic dynamics. It is suggested these field scaled tests use a rotor at a larger scale in order to alleviate the Reynolds number effects that would be highly exaggerated in a 1% model. Such work is underway in the form of a 20% scale Segmented Ultralight Morphing Rotor-Demonstrator for ground, parked, and operational testing [45–47]. Additionally, the success in using additive manufacturing with a structurally optimized bio-inspired design is suggested to be further explored for full-scale blades as an option to reduce blade mass while maintaining structural stiffness. Finally, while this study investigates the flap-wise blade performance in terms of structural response, alternate scaling models are proposed to explore the edgewise fatigue or design failures such as panels cracking or leading edge erosion as these are often the design drivers in extreme-scale turbines.

Declaration of competing interest

The authors declare that they have no known competing financial interests or personal relationships that could have appeared to influence the work reported in this paper.

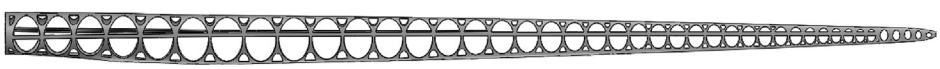

Fig. 11. The top view of the blade structure of the Version 5CF 1% GAS SNL100-03 blade model.

Please cite this article as: M. Kaminski et al., Ground testing of a 1% gravo-aeroelastically scaled additively-manufactured wind turbine blade with bio-inspired structural design, Renewable Energy, https://doi.org/10.1016/j.renene.2019.10.152

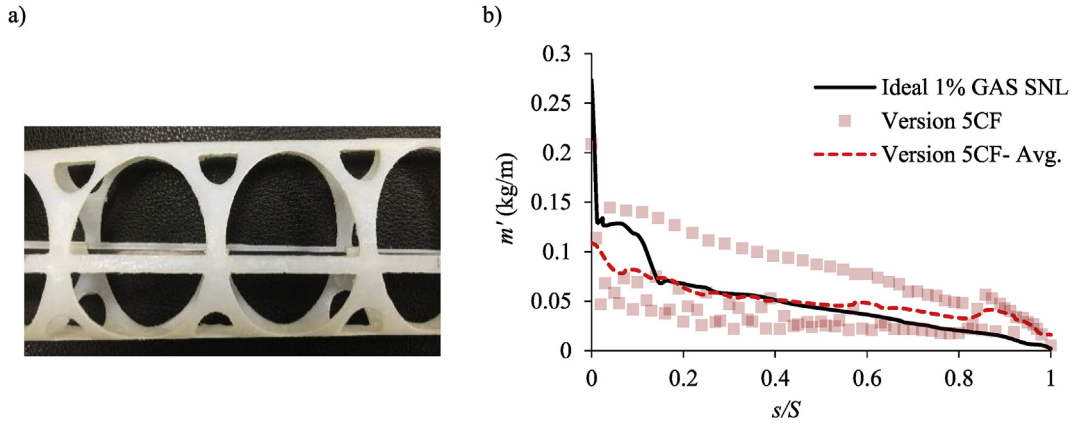

Fig. 12. Version 5CF blade showing: a) the organic structure and b) discrete and smoothed linear mass density along the span as compared to the ideal 1% GAS SNL100-03 blade.

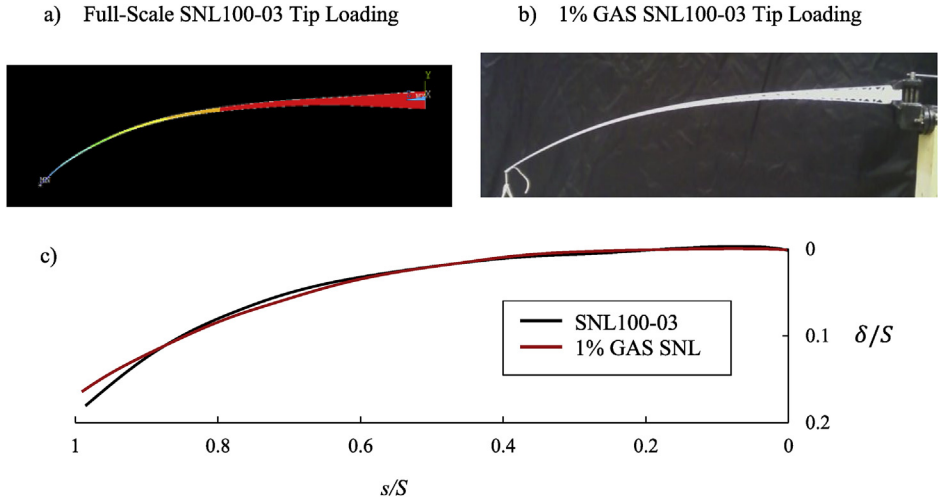

Fig. 13. Blade deflection under a steady-state flap-wise load equivalent to average load for rated conditions: a) ANSYS predictions of the full-scale SNL100−03, b) fabricated 1% GAS SNL100-03 blade, and c) a quantitative comparison of non-dimensional deflections.

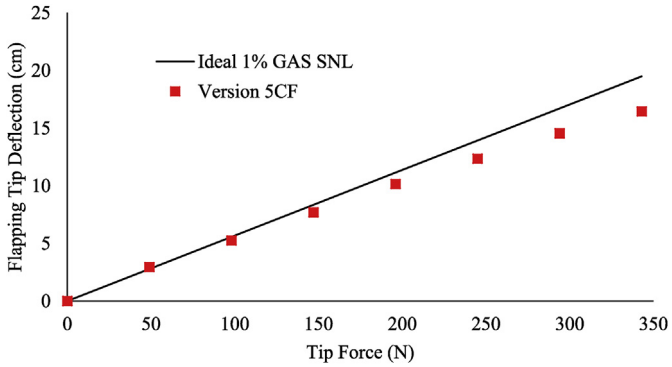

Fig. 14. The flap-wise tip deflections of the 1% GAS SNL100-03 Version 5CF blade (red squares) compared to ideal scaled model (black line). (For interpretation of the references to colour in this figure legend, the reader is referred to the Web version of this article.)

Acknowledgements

The authors would like to acknowledge the Rapid Prototyping Lab and Dwight Dart at the University of Virginia for providing the tools and assistance needed to additively manufacture the 1% blades. The authors would also like to acknowledge the remainder of the ARPA-E Segmented Ultra-Light Morphing Rotor (SUMR) team for comments and suggestions throughout the research study. This work has been supported by ARPA-E under award number DE-AR0000667. Any opinions, findings, and conclusions or recommendations expressed in this material are those of the authors and do not necessarily reflect the views of ARPA-E.

References

[1] U.S. Department of Energy (DOE), Wind Vision. A New Era for Wind Power in the United States, 2015, p. 350. DOE/GO-102015-4557.
[2] U.S. Energy Information Administration, Annual energy outlook 2015, Off. Integr. Int. Energy Anal. 1 (2015) 1−244. DOE/EIA-0383(2013).
[3] D.T. Griffith, T.D. Ashwill, The Sandia 100-meter all-glass baseline wind turbine Blade : SNL100-00, Baseline 1−67 (2011). Report No. SAND2011-3779.
[4] D.T. Griffith, The SNL100-01 Blade: Carbon Design Studies for the Sandia 100-meter Blade, Sand2013-1178, 2013, pp. 1−26.
[5] D.T. Griffith, The SNL100-02 Blade : Advanced Core Material Design Studies for the Sandia 100- Meter Blade, Sand2013-10162, 2013.
[6] D.T. Griffith, P.W. Richards, The SNL100-03 Blade : Design Studies with Flatback Airfoils for the Sandia 100-meter Blade, 2014.
[7] C. Noyes, C. Qin, E. Loth, Pre-aligned downwind rotor for a 13.2 MW wind turbine, Renew. Energy 116 (2018) 749−754, https://doi.org/10.1016/j.renene.2017.10.019.
[8] L. Bergami, H. Madsen, A Two-Bladed Teetering Hub configuration for the DTU 10 MW RWT: loads considerations, Eur. Wind Energy. (2014) 1−8.
[9] A.M. Viselli, A.J. Goupee, H.J. Dagher, Model test of a 1:8-scale floating wind turbine offshore in the gulf of Maine, J. Offshore Mech. Arct. Eng. (2015),

https://doi.org/10.1115/1.4030381.
[10] J.D. Singleton, W.T. Yeager, Important scaling parameters for testing model-scale helicopter rotors, J. Aircr. 37 (2000) 396–402, https://doi.org/10.2514/2.2639.
[11] Z. Wan, C.E.S. Cesnik, Geometrically nonlinear aeroelastic scaling for very flexible aircraft, in: 54th AIAA/ASME/ASCE/AHS/ASC Struct. Struct. Dyn. Mater. Conf., Boston, 2013, pp. 1–10, https://doi.org/10.2514/6.2013-1894.
[12] A. Jain, A. Robertson, J. Jonkman, A.J. Goupee, R. Kimball, A.H. Swift, FAST code verification of scaling laws for DeepCwind floating wind system tests, Proc. Twenty Sec. Int. Offshore Polar Eng. Conf. 4 (2012) 355–365.
[13] F. Campagnolo, C.L. Bottasso, P. Bettini, Design, manufacturing and characterization of aero-elastically scaled wind turbine blades for testing active and passive load alleviation techniques within a ABL wind tunnel, J. Phys. Conf. Ser. 524 (2014), https://doi.org/10.1088/1742-6596/524/1/012061.
[14] W. Du, Y. Zhao, Y. He, Y. Liu, Design, analysis and test of a model turbine blade for a wave basin test of floating wind turbines, Renew. Energy 97 (2016) 414–421, https://doi.org/10.1016/j.renene.2016.06.008.
[15] A.N. Robertson, J.M. Jonkman, A.J. Goupee, A.J. Coulling, J. Browning, M.D. Masciola, P. Molta, Summary of Conclusions and Recommendations Drawn from the DeepCwind Scaled Floating Offshore Wind System Test Campaign, 2013.
[16] E. Loth, M. Kaminski, C. Qin, Gravo - aeroelastic scaling for extreme - scale wind turbines, AIAA Aviat. Conf. (2017) 1–11.
[17] M. Kaminski, E. Loth, C. Qin, D.T. Griffith, G. Scaling, Gravo-aeroelastic scaling a 13.2 MW wind turbine blade to a 1-meter model, AIAA SciTech. (2018) 1–12.
[18] al W.Z. Shen, V.A.K. Zakkam, J.N. Sørensen, Y. Jiang, S. Liu, D. Zhao, H. Canet, P. Bortolotti, C. Bottasso, Gravo-aeroelastic Scaling of Very Large Wind Turbines to Wind Tunnel Size, 2018, p. 42006, https://doi.org/10.1088/1742-6596/1037/4/042006.
[19] N. Aage, E. Andreassen, S. Lazarov, O. Sigmund, Giga-voxel computational morphogenesis for structural design, Nat. Publ. Gr. 550 (2017), https://doi.org/10.1038/nature23911.
[20] J. Wolff, The Law of Bone Remodelling, Springer, 1986.
[21] B. Thierry, M. Singh, W. Kaumanns, Who's Afraid of the Big Bad Wolff?: "Wolff's Law" and Bone Funcational Adaptation, vol 1, Cambridge Univ. Press, New York, 2004, pp. 80–83, https://doi.org/10.1002/ajpa.
[22] B. Campbell, Thomas Williams, Christopher Ivanova, Olga Garrett, Could 3D Printing Change the World? Technologies, Potential, and Implications of Additive Manufacturing, 2011, pp. 3–7.
[23] More than 3D printing, Design. Mater. Prod. (2017). https://svn.mpia.de/trac/gulli/att/raw-attachment/wiki/AlteVortraege2017S1/2017-05-19_3DDruck.pdf.
[24] P.J. Bishop, S.A. Hocknull, C.J. Clemente, J.R. Hutchinson, A.A. Farke, B.R. Beck, R.S. Barrett, D.G. Lloyd, Cancellous bone and theropod dinosaur locomotion. Part I—an examination of cancellous bone architecture in the hindlimb bones of theropods, PeerJ (2018), https://doi.org/10.7717/peerj.5778.
[25] K.J.A. Brookes, Europe salutes metal-based, AM Met. Powder Rep. 73 (2018) 119–125, https://doi.org/10.1016/j.mprp.2018.02.004.
[26] M. Make, G. Vaz, Analyzing scaling effects on offshore wind turbines using CFD, Renew. Energy 83 (2015) 1326–1340, https://doi.org/10.1016/j.renene.2015.05.048.
[27] H.R. Martin, R.W. Kimball, A.M. Viselli, A.J. Goupee, Methodology for Wind/Wave Basin Testing of Floating Offshore Wind Turbines, 2014, https://doi.org/10.1115/1.4025030.
[28] L. Li, Y. Gao, Z. Hu, Z. Yuan, S. Day, H. Li, Model test research of a semi-submersible floating wind turbine with an improved deficient thrust force correction approach, Renew. Energy 119 (2018) 95–105, https://doi.org/10.1016/j.renene.2017.12.019.
[29] A. Barker, G. Timco, H. Gravesen, P. Vølund, Ice loading on Danish wind turbines. Part 1: dynamic model tests, Cold Reg. Sci. Technol. 41 (2005) 1–23, https://doi.org/10.1016/j.coldregions.2004.05.002.
[30] B.K. Post, R.F. Lind, P.D. Lloyd, V. Kunc, J.M. Linhal, L.J. Love, The economics of big area additive manufacturing, Proc. Solid Free. Fabr. Symp. (2016) 1176–1182.
[31] N. Guo, M.C. Leu, Additive manufacturing: technology, applications and research needs, Front. Mech. Eng. 8 (2013) 215–243, https://doi.org/10.1007/s11465-013-0248-8.
[32] Stratasys, Digital Materials Data Sheet, 2000.
[33] The composites store, n.d, http://www.cstsales.com/.
[34] GLAD cling wrap, n.d, https://www.glad.com/food-storage/plastic-wrap/clingwrap/.
[35] J. Foreman, P.S. Gill, S.R. Sauerbrunn, Tensile Modulus of Plastic Films, (n.d).
[36] Q.Q. Liang1, Y.M. Xie1, G.P. Steven2, Optimal Selection of Topologies for the Minimum-Weight Design of Continuum Structures with Stress Constraints, ((n.d.)).
[37] N. Aulig, M. Olhofer, Evolutionary Computation for Topology Optimization of Mechanical Structures: an Overview of Representations, ((n.d.)).
[38] 2 - Blades (Carbon Fibre), 1 . 8 Metre Diameter & Induction Motor to PMA Conversion, ((n.d.)).
[39] P. Jamieson, Innovation in Wind Turbine Design, First, Wiley, 2011.
[40] E. Loth, A. Steele, B. Ichter, M. Selig, P. Moriarty, Segmented Ultralight pre - aligned rotor for extreme - scale wind turbines, in: AIAA Aerosp. Sci. Meet., Nashville, 2012.
[41] A. Pourrajabian, P.A. Nazmi Afshar, M. Ahmadizadeh, D. Wood, Aero-structural design and optimization of a small wind turbine blade, Renew. Energy (2016), https://doi.org/10.1016/j.renene.2015.09.002.
[42] S.R. Wakayama, Lifting Surface Design Using Multidisciplinary Optimization, 1995.
[43] M.D. Motok, Stress concentration on the contour of a plate opening of an arbitrary corner radius of curvature, Mar. Struct. (1997), https://doi.org/10.1016/s0951-8339(96)00012-3.
[44] N. Gaudern, A practical study of the aerodynamic impact of wind turbine blade leading edge erosion, J. Phys. Conf. Ser. (2014), https://doi.org/10.1088/1742-6596/524/1/012031.
[45] G.K. Ananda, S. Bansal, M.S. Selig, Aerodynamic Design of the 13.2 MW SUMR-13i Wind Turbine Rotor, 2018, https://doi.org/10.2514/6.2018-0994.
[46] C.J. Bay, R. Damiani, L. Jay Fingersh, S. Hughes, M. Chetan, S. Yao, D. Todd Griffith, G.K. Ananda, M.S. Selig, D.S. Zalkind, L.Y. Pao, D. Martin, K.E. Johnson, M. Kaminski, E. Loth, Design and testing of a scaled demonstrator turbine at the national wind technology center, n.d, https://arc.aiaa.org/doi/pdf/10.2514/6.2019-1068. (Accessed 21 January 2019).
[47] S. Yao, D. Todd Griffith, M. Chetan, C.J. Bay, R. Damiani, M. Kaminski, E. Loth, Structural Design of a 1/5 Th Scale Gravo-Aeroelastically Scaled Wind Turbine Demonstrator Blade for Field Testing, (n.d.). doi:10.2514/6.2019-1067.

Please cite this article as: M. Kaminski et al., Ground testing of a 1% gravo-aeroelastically scaled additively-manufactured wind turbine blade with bio-inspired structural design, Renewable Energy, https://doi.org/10.1016/j.renene.2019.10.152